Available online at www.sciencedirect.com

ScienceDirect

Procedia Structural Integrity 28 (2020) 2157–2167

Structural Integrity Procedia

www.elsevier.com/locate/procedia

1st Virtual European Conference on Fracture

Experimental evaluation of relaxed strains in a pipe-to-plate welded joint by means of incremental cutting process

A. Chiocca*, F. Frendo, L. Bertini

University of Pisa, Department of Civil and Industrial Engineering, Largo Lucio Lazzarino 2, Pisa 56123, Italy

Abstract

Residual stresses play a major role in the fatigue life and static strength of welded components. The high thermal gradient to which the material is subjected to during welding often leads to tensile residual stresses in critical notched regions. Residual stresses evaluation is crucial as they can cause unexpected failures or premature degradation of components, thus shortening the service life. Since determining their magnitude a priori is challenging, the experimental evaluation is fundamental when tensile residual stresses could be degrading for a component. The assessment of residual stresses can be performed through different techniques, all involving indirect measurements based on the detection of elastic deformation or displacement. In this context, a method belonging to the sectioning method category is proposed to calculate relaxed strains in a pipe-to-plate welded joint. The relaxed strains are determined by means of strain gauges placed on the upper surface of the plate nearby the weld bead. The results thus obtained represent strains measurements generated after an incremental hole cutting process performed on the bottom surface of the plate, opposite respect to the surface where the strain gauges were attached. Through this method, the calculated strains are related to the diameter and depth of the performed hole, as well as the location where the strain gauges are placed on the plate surface.

Keywords: Relaxed strain; welded joint; incremental hole cutting; experimental measures; residual stress

1. Introduction

Residual stresses are often the cause of unforeseen failures and dimensional irregularities, as they can reduce the strain resistance [7], fatigue life [1] and promoting stress-corrosion failures [17]. Especially residual tensile stresses can be degrading for a mechanical component shortening the fatigue life due to early crack initiation and faster crack propagation [12]. This is especially the case of welded joints, where residual stresses are generally produced because of the high thermal gradient caused by the welding process. Steep stress gradients are generated around the weld

* Corresponding author. Tel.: +39-050-221-8011.
E-mail address: andrea.chiocca@phd.unipi.it

10.1016/j.prostr.2020.11.043

bead leading in highly conservative assumptions in standard codes, often due to the lack of knowledge on the effect of residual stresses for the material [8]. The knowledge of residual stresses is often required to perform a reliable fatigue assessment, as welding tensile residual stress is detrimental for the fatigue life and fatigue strength of welded joints [16]. On the contrary, compressive residual stresses are sometimes introduced to strengthen a component (e.g. shot peening and plastic deformation in automotive helical springs [2]).
Several methods exist to evaluate residual stresses, each one with different issues and all belonging to the research field of inverse problems [15, 11]. Some methods introduce additional damage to the component and are based on the detection of elastic deformation or displacement due to stressed material relieving. Among these methods, they can be mentioned destructive techniques as the sectioning method [21] or semi-destructive techniques as the hole drilling method [20]. Alternatively, non-destructive techniques can be employed, mainly for periodic inspection routines; these are mainly based on neutron diffraction [20] or ultrasound [19, 18] technologies.
This work is the continuation of early-stage experimental research on residual stresses, already discussed by the authors [6]. An experimental investigation of relaxed strains (ε_R) in a welded pipe-to-plate joint is presented in the following. Relaxed strains were calculated as a result of stresses relieving within the specimen caused by a material removal process involving a significant volume of the specimen. The strain measurements were performed by means of strain gauges placed on the plate surface close to the weld toe, while the incremental cutting process was performed on the plate's bottom surface. The material removal from the bottom surface is carried out in such a location and a manner that stresses are released close to the area of interest. The plate upper surface allows strain measurements through the easy placement of strain gauges besides being the area of the specimen which is most affected by residual stress redistribution caused by the cutting process.

2. Material and model

A pipe-to-plate welded joint has been studied in the following work. The specimen, shown in Figure 1, consisted of a tube strengthened by an internal circular plate and subsequently welded to a base plate by means of gas metal arc welding (GMAW). The specimens were entirely manufactured from S355JR structural steel, while, the parameters adopted during welding are presented in Table 1. Material and components employed in this work are widely adopted in the railway sector for high-speed trains, as already shown by [14]. Seize-wise, the tube is 44 mm of internal diameter with a thickness of 10 mm, whereas the plate, is quadrangular, 190 mm side and 25 mm thick. The four holes on the plate were drilled to fix the specimen on the fatigue test bench (not discussed in this work); similarly, the internal chamber generated by the circular support was pressurized to detect any through-the-thickness crack during fatigue tests [3, 4, 9, 10].
The welding process led specifically to a non-full penetration weld bead, as shown in Figure 1 b). An important consideration derived from the different radii dimensions between weld toes and root, that can be observed in Figure 1. Due to the gravitational effect on the molten metal during the welding process, the upper weld toe had a much larger radius (i.e. 2 mm) if compared to to the weld root and the lower weld toe radii (i.e. 0.2 mm). It is worth noting that a stress concentration was expected in all the existing notches, nevertheless, the experimental strain measurements were located in the surrounding area of the weld bead on the flange surface where higher stress gradients were expected. The weld root area was technically unsuitable for residual stress measurement, for this reason only the outer region on flange surface surrounding the weld bead has been considered.

Table 1. Welding process parameters

Welding Current (*I*)	**Arc Voltage (*U*)**	**Welding Time**	**Welding Speed**
211 A	25 V	75 s	2.7 mm s^{-1}
Filler material	**Welding wire diameter**	**Shielding gas**	**Gas flowrate**
G3/4 Si1	1.20 mm	82% Ar 18% CO_2	0.62 m^3 h^{-1}

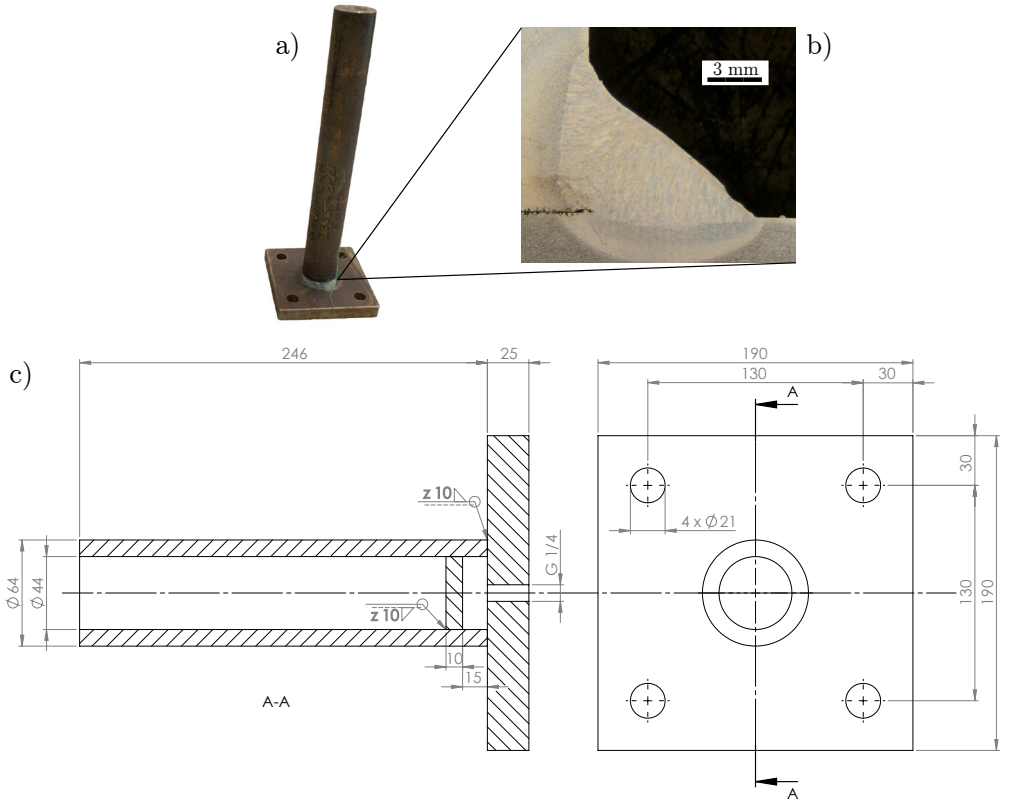

Fig. 1. Real sample (**a**), micrograph of the weld seam (**b**), technical drawing of the specimen (**c**) from [5]

3. Relaxed strain measurements

Several strain measurements around the weld bead have been obtained through strain gauges by means of an incremental hole cutting process, starting from the bottom of the base plate. The drilling process was required to relieve the specimens, as the strain gauges were installed after completion of the welding process. This procedure, schematically illustrated in Figure 2, is meant to achieve experimental relaxed strains, representative of the residual stress state in the weld region close to the weld toe.

Linear strain gauges with nominal resistance of 120 Ω and measuring grid length of 0.6 mm and 1.5 mm were employed together with the *Model 5100B Scanner* data acquisition system from StrainSmart®. The largest strain gauges with a grid length of 1.5 mm have been placed with rather large angular steps during installation ($\Delta\theta > 15°$). On the contrary, the 0.6 mm grid length were specifically used for localized strain measurements, with an angular step of $\Delta\theta = 6°$ and located in the area opposite at the welding starting point.

The cutting process was step-based to control the acquired results of strains and achieve different measures for different cutting depth (δ) and holes' diameter (d). Figure 2 shows, on the left side, two holes dimensions employed together with the hole depth parameter δ. Overall, the represented holes in Figure 2 refer to the following diameters: $d = 42$ mm in dark grey and $d = 100$ mm in orange. It is worth noting that no detectable measurements were obtained from the 42 mm hole since the calculated relaxed strain magnitude was of the same order of magnitude of the experimental noise. A picture of the machining process is shown in Figure 3, in which the placement of the specimen on the milling machine and the machining of the hole are shown. Figure 3 illustrates how the outer flange edges and the tube were machined to sufficiently compact the specimen to perform the installation. All pre-testing machining operations were performed on specimen's regions with a negligible residual stress state, thus to not affect the area of interest close to the weld bead. The drilling was carried out through a milling cutter with a fixed tool position and specimen rotation. From a procedural standpoint, while the milling cutter tool was maintained at a constant depth, the hole

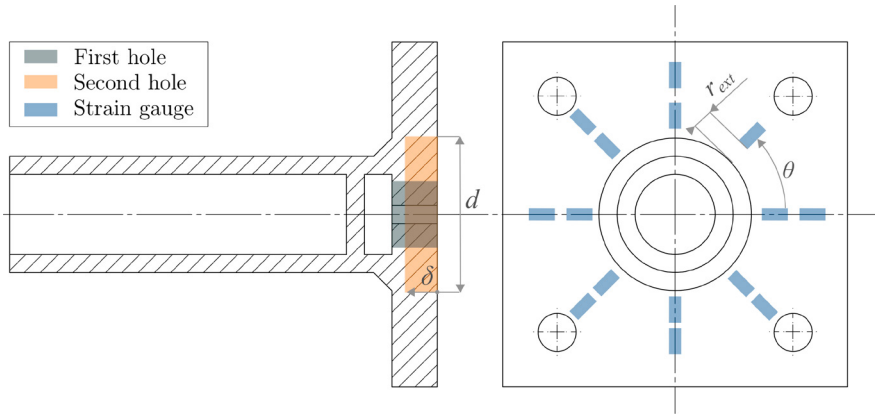

Fig. 2. Outline of the incremental hole cutting process.

diameter was increased by 5 mm after each complete rotation of the specimen. The process continued until the desired diameter was reached, thereafter the tool's depth was increased and the process reiterated. Each complete rotation is followed by a machining interruption, as the specimen shall be returned to the starting position due to cabling issues.

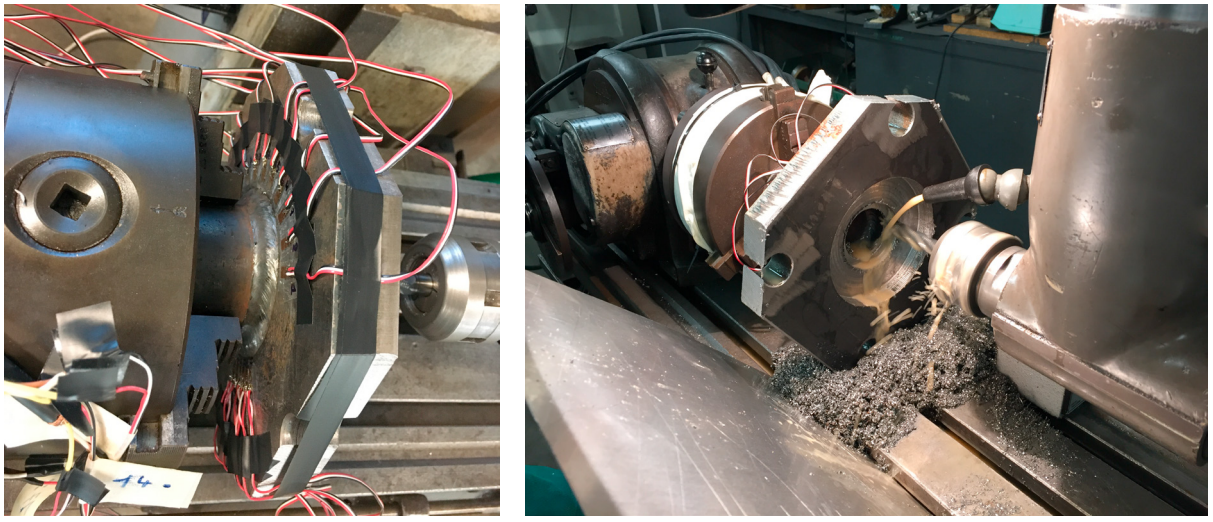

Fig. 3. Experimental machining of the specimen's plate, front (left) and back (right) views

The strain gauges were placed according to the pattern in Figure 2, where r_{ext} and θ identified respectively, the radial distance between the strain gauge and the weld toe, and the angular distance from the starting welding point and the strain gauge. The welding starting point is identified as the position where the welding process begins and ends. It is worth noting that in this particular position the material is affected by a double thermal process which may cause a significant variation in residual stress and strain values, possibly leading to a symmetry-break in the stress and strain results in the hoop direction.

Table 2 shows the information of the tested specimen, specifically reporting the main parameters r_{ext} and the angular steps $\Delta\theta$ employed during strain gauges placement. The specimen *Test-5* was heat-treated after welding (i.e. 650° for 1 hour and cooled down gradually to ambient temperature) with the purpose to corroborate the strain gauges measurements through comparison between the as-welded condition and the annealed one. An overview of strain gauges placement on the flange surface is given in Figure 4, specifically the *Test-1* and *Test-3* specimen.

The incremental hole cutting process is a step-based method and allows strain measurements to be determined de-

pending on several parameters. From the placement of a single strain gauge, measurements as a function of r_{ext}, θ, δ and d can be obtained, where r_{ext} and θ remain fixed while δ and d vary during the cutting process

$$\varepsilon_{rr} = f(r_{ext}, \theta, \delta, d)$$

Table 2. Set-up information of the experimental tests for relaxed strains measurements

Name	Heat treatment	Strain gauges num.	r_{ext} (mm)	$\Delta\theta$ (°)
Test-1	/	8	6.5/9/13	90° steps
Test-2	/	6	6.5/9/13	90° steps
Test-3	/	12	6.5	30° steps
Test-4	/	19	6.5	15°/6° steps
Test-5	annealing	12	6.5	30° steps

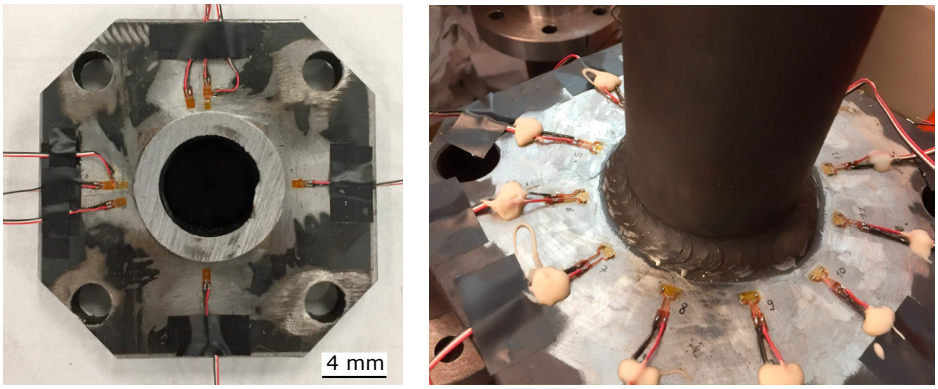

Fig. 4. *Test-1* specimen (left), with eight strain gauges applied at a 90° step angle. *Test-3* specimen (right) with twelve applied strain gages with 30° step angles

4. Results and discussion

The following section presents an exploratory data analysis of the collected experimental results, together with a discussion. This section is aimed at obtaining a clear understanding of the relaxed strain behaviour concerning the coordinates that define the strain gauge positioning on the flange surface (i.e. r_{ext} and θ). Table 3 shows the complete data set of all results collected during experimental tests. All data were collected for a hole diameter of 100 mm and for different r_{ext} and θ values. Since the cutting was performed by incremental steps of 5 mm, δ assumes discrete values of 5 mm, 10 mm, 15 mm and 20 mm respectively. The strain gauges were mainly positioned close to the weld seam, as the stress-strain gradient increases when approaching the weld toe. This is why, in Table 3 the majority of strain gauge readings refer to $r_{ext} = 6.5$ mm, distance which is a compromise between feasibility in strain gauge installation and vicinity to the weld notch. As expected, the results show that the strain gauge readings for the heat-treated specimen (*Test-5*) results in a decrease of an order of magnitude compare to the as-welded condition specimens.
Measurements obtained over a small arc of circumference (i.e. Figure 5), carried out using 0.6 mm grid length strain gauges, allowed to evaluate the variation on the ε_{Rrr} due to local weld bead geometry. Strain gauges have been positioned in the furthest location respect the welding starting point to avoid any influence from the double thermal cycle that the material undergoes in this area. The measurements obtained for different δ show a similar pattern, as confirmed by the rather constant standard deviation. However, expecting in this location a constant ε_{Rrr} over the hoop

coordinate[1], the variability can be mainly explained by the uneven geometry of the weld bead. A standard deviation of 67% relative to the mean value of six strain gauges was found for $\delta = 5$ mm. This demonstrates how, although the region around the weld bead is interesting from a measurement standpoint, it is also most affected by the uneven geometry of the weld notch. The irregular geometry further contributes to a non-axisymmetric residual stress field and leaves residual stresses highly dependent on a parameter hardly controllable during the production phase.
Figure 6 shows a data processing of the as-welded specimens presented in Table 3. Specifically, relaxed radial strains (ε_{Rrr}) are displayed for three radial coordinates (i.e. $r_{ext} = 6.5\,\text{mm}, 9\,\text{mm}, 13\,\text{mm}$) through mean value and standard deviation. The four graphs illustrate respectively the four steps adopted during the cutting process and demonstrate how radial relaxed strains globally increase, while increase the hole depth value. It is worth noting that the graphs are presented on different scales as ε_{Rrr} varies in magnitude, ranging from $\approx 10^{-4}$ for $\delta = 5$ mm to $\approx 10^{-3}$ for $\delta = 20$ mm. Further important information resulting from Figure 6 lies in the symmetric consistency of relaxed strains. Indeed, it is evident that all results present a fairly considerable standard deviation, indicating that the strain range and therefore the stress range is most likely not axisymmetric. This outcome suggests that the welding process, and therefore the stresses generated from it, are a strictly three-dimensional phenomenon. It is therefore important to pay attention when the process is modelled based on a two-dimensional hypothesis, such as axial symmetry, plane stress or plane strain. As a matter of fact, the goodness of the results is not known in advance and there may even be the chance of obtaining non-conservative solutions. It is well known that the residual stress field increases when approaching a notch (i.e. weld toe or weld root), as clearly detectable by using the hot spot stress evaluation methods on welded T-joint [13]. Despite this, relaxed strains have seemingly unusual behaviour, as can be seen from Figure 6. This characteristic trend can be explained by considering two effects playing a role during the cutting process, a general bending and local skin effects as shown in the cross-sectional view of Figure 7 . The incremental hole cutting at the bottom of the plate allows the upper part to bend due to the release of residual stresses, therefore, stresses and strains decrease around the weld seam. On the contrary, the weld bead shrinkage generates a skin-positive radial strain which increases closer to the weld toe, generating a monotonous growing strain function as r_{ext} approaches zero.

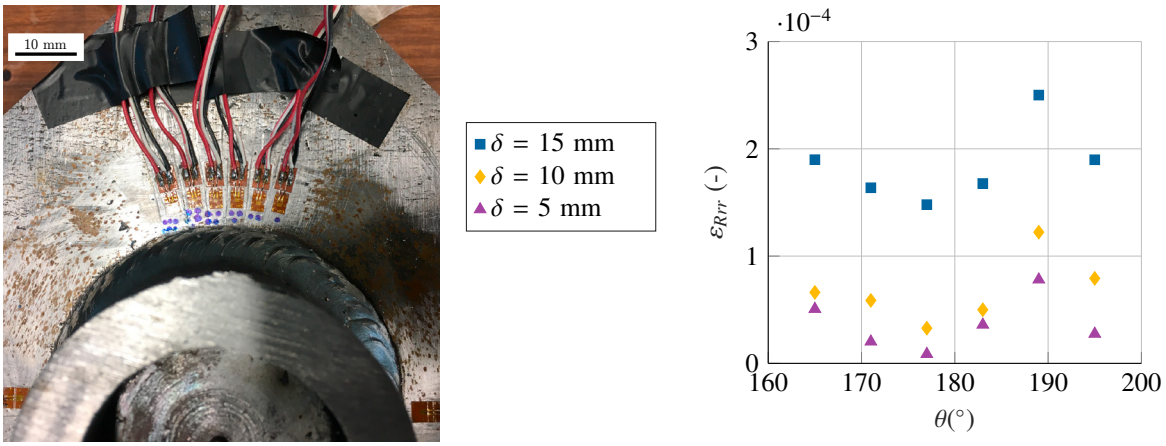

Fig. 5. Strain gauge positioning on the plate surface (left) and relaxed radial strain measurements over angular coordinate (right)

The combination of these features produces the behaviour shown in Figure 6, specifically, for the depth of pass up to $\delta = 15$ mm the plate bending prevails while for $\delta = 20$ mm the two effects stabilize leading to an increase in the strain gradient in the proximity of the weld bead. Furthermore, the experimental data from Table 3 are presented as a function of θ, as shown in Figure 8. For the sake of clarity, relaxed radial strain results belonging to similar θ values (i.e. $\pm 5°$) are grouped through their mean value for both ε and θ. Two different charts were adopted as a result of the large variation in the data magnitude. For small δ values the measurement sensitivity might be blurred by the background noise, as in some cases negative relaxed strain values have been calculated. Besides, for ease of reading,

[1] The symmetric specimen's geometry, material isotropy and the constant heat transfer during the welding process are supposed to result in a constant residual stress behaviour

the mean value of relaxed strains have been reported for different depths of pass through dashed lines. Again, it is clear a ε_{Rrr} variation over the hoop coordinate θ. However, in this case, a common behaviour between data can be observed since ε_{Rrr} slightly increases getting closer to the welding starting point $\theta = 0°$.

Table 3. Summary of experimental relaxed strains measurements in **bold** ($\mu\varepsilon$) for the 100 mm diameter hole

Test-1 (as welded)

θ (°)	r_{ext} (*mm*)	δ (*mm*)			
		5	10	15	20
0	6.5	/	**281**	**652**	**3299**
0	13	/	**298**	**482**	**408**
5	6.5	/	**460**	**577**	**1114**
90	9	/	**233**	**440**	**2143**
180	9	/	**297**	**600**	**836**
270	6.5	/	**236**	**337**	**1360**
270	13	/	**294**	**274**	**270**
275	6.5	/	**248**	**307**	**760**

Test-2 (as welded)

θ (°)	r_{ext} (*mm*)	δ (*mm*)			
		5	10	15	20
0	9	**99**	**262**	**538**	**993**
90	6.5	**18**	**137**	**298**	**3021**
90	13	**75**	**220**	**456**	**500**
180	6.5	**-5**	**95**	**256**	**1961**
180	13	**85**	**242**	**447**	**575**
270	9	**60**	**222**	**296**	**466**

Test-3 (as welded)

θ (°)	r_{ext} (*mm*)	δ (*mm*)			
		5	10	15	20
0	6.5	**28**	**165**	**329**	**1556**
30	6.5	**65**	**184**	**332**	**1720**
60	6.5	**0**	**135**	**204**	**770**
90	6.5	**4**	**163**	**255**	**972**
120	6.5	**12**	**148**	**224**	**1090**
150	6.5	**19**	**144**	**245**	**1496**
180	6.5	**13**	**145**	**285**	**1926**
210	6.5	**15**	**142**	**309**	**2281**
240	6.5	**7**	**113**	**262**	**2170**
270	6.5	**-3**	**109**	**260**	**2090**
300	6.5	**-17**	**96**	**190**	**1997**
330	6.5	**-32**	**85**	**49**	**564**

Test-4 (as welded)

θ (°)	r_{ext} (*mm*)	δ (*mm*)			
		5	10	15	20
0	6.5	**92**	**182**	**366**	/
15	6.5	**40**	**113**	**279**	/
30	6.5	**15**	**59**	**190**	/
45	6.5	**-4**	**12**	**129**	/
60	6.5	**-20**	**-33**	**99**	/
75	6.5	**-11**	**-34**	**107**	/
90	6.5	**-12**	**-32**	**99**	/
165	6.5	**51**	**66**	**190**	/
171	6.5	**20**	**59**	**164**	/
177	6.5	**9**	**33**	**148**	/
183	6.5	**36**	**50**	**168**	/
189	6.5	**78**	**122**	**250**	/
195	6.5	**27**	**79**	**190**	/
270	6.5	**9**	**99**	**202**	/
285	6.5	**14**	**93**	**202**	/
300	6.5	**26**	**124**	**221**	/
315	6.5	**53**	**94**	**181**	/
330	6.5	**87**	**132**	**251**	/
345	6.5	**148**	**222**	**400**	/

Test-5 (annealed)

θ (°)	r_{ext} (*mm*)	δ (*mm*)			
		5	10	15	20
0	6.5	**-4**	**-2**	**1**	**-279**
30	6.5	**-27**	**-28**	**-38**	**20**
60	6.5	**-37**	**-43**	**-54**	**-62**
90	6.5	**-12**	**-17**	**-11**	**492**
120	6.5	**-22**	**-30**	**-22**	**-29**
150	6.5	**-28**	**-42**	**-32**	**597**
180	6.5	**-31**	**-17**	**-7**	**386**
210	6.5	**-32**	**-33**	**-46**	**493**
240	6.5	**-23**	**-9**	**-23**	**205**
270	6.5	**-8**	**12**	**4**	**273**
300	6.5	**-10**	**2**	**-6**	**147**
330	6.5	**-2**	**-6**	**23**	**263**

The variation of data around the mean value can be explained by the inherent variation in the thermal load due to the welding process. During welding, the stress and strain fields in the specimen are strongly non-axisymmetric, resulting in behaviour after welding as the one shown in Figure 8. Besides, in the starting and ending point of the welding process, the material is subjected to a double thermal process that leads the solution in that area far from the one achievable by an axisymmetric model.

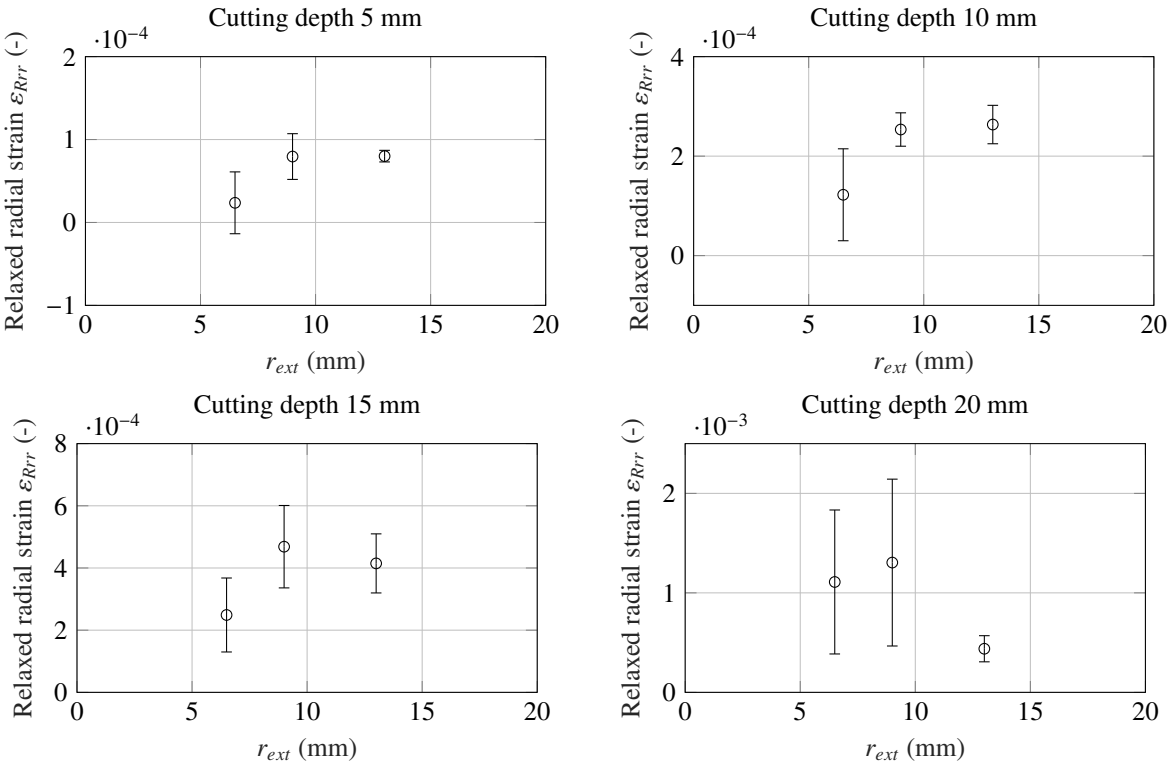

Fig. 6. Relaxed radial strain over radial distance from the weld toe. The results are presented through mean value and standard deviation

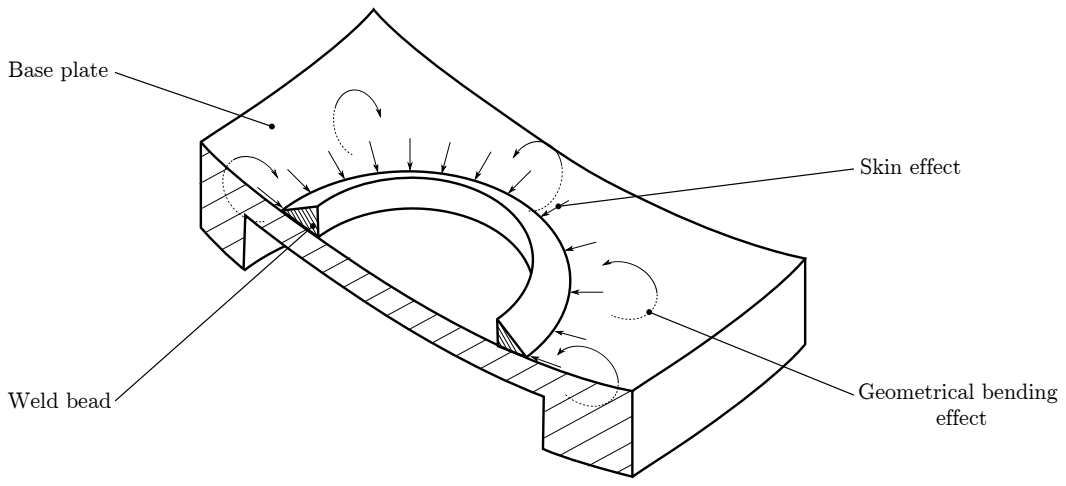

Fig. 7. Cross-sectional view of the base plate and weld bead with outlined the bending and skin effects due to the incremental cutting process

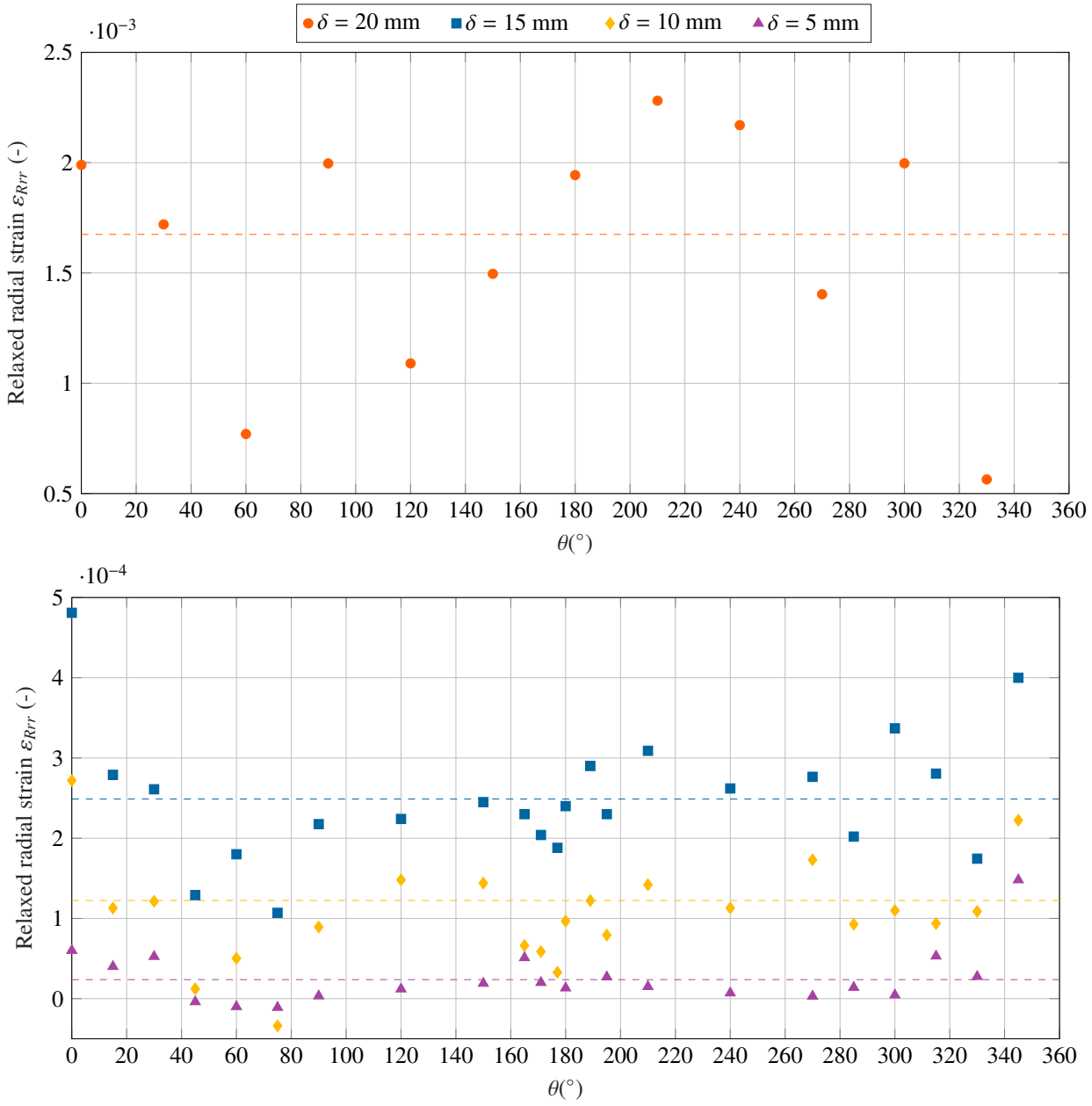

Fig. 8. Relaxed radial strain over specimen hoop coordinate for different cutting depths and a fixed strain gauge radial distance of $r_{ext} = 6.5$ mm. The mean value are represented as dashed lines for each depth of pass δ

5. Conclusions

From the research carried out and from the results obtained it can be concluded that:

- the incremental hole drilling process allows obtaining an extensive number of measurements for every strain gauge employed through parameters variation such as hole diameter and depth;

- the highly stressed areas close to the weld bead can be reached by the appropriate application of properly dimensioned strain gauges; ideally, the smaller the size of the strain gauge, the smaller the distance to the weld notches that can be reached;
- strain gauge measurements clearly show that the welding process is a three-dimensional phenomenon; assume the welding process as two-dimensional can be doubtful since in locations such as the welding starting point the material undergoes an important thermal process more than once;
- residual stresses can be obtained based on a numerical model that represents the welding process and the incremental hole cutting procedure; relaxed strains results can be used to calibrate the numerical model and obtain more accurate residual stress results;
- experimental measurements of residual stresses are still challenging today because of the poor repeatability of results; therefore, although residual stresses are very useful to have a broad comprehension of the state of material after welding, a comparison with numerical or analytical data is still necessary;

It is possible to outline a feasible development regarding this experimental procedure. Generally speaking, residual stresses can be computed by comparing experimental results with numerical or analytical models. The determination of residual stresses is inherently indirect since the determination of another quantity is firstly needed. If required, the value of residual stresses can be obtained by direct comparison of experimental and numerical measurements of relaxed strains. A numerical model can be developed and fine-tuned by means of experimental data, thus to simulate the welding process and the subsequent cutting process. Once the validity of the numerical model has been verified by comparison with relaxed strain results, residual stresses can be directly calculated starting from the numerical model itself. In this case, relaxed strains behave like the indirect parameter that needs to be measured to obtain residual stresses.

References

[1] Barsoum, Z., Barsoum, I., 2009. Residual stress effects on fatigue life of welded structures using LEFM. Engineering Failure Analysis 16, 449 – 467. doi:10.1016/j.engfailanal.2008.06.017.

[2] Bartolozzi, R., Frendo, F., 2011. Stiffness and strength aspects in the design of automotive coil springs for McPherson front suspensions: a case study. Proceedings of the Institution of Mechanical Engineers, Part D: Journal of Automobile Engineering 225, 1377–1391. doi:10.1177/0954407011403853.

[3] Bertini, L., Cera, A., Frendo, F., 2014. Experimental investigation of the fatigue resistance of pipe-to-plate welded connections under bending, torsion and mixed mode loading. International Journal of Fatigue 68, 178–185. doi:10.1016/j.ijfatigue.2014.05.005.

[4] Bertini, L., Frendo, F., Marulo, G., 2016. Effects of plate stiffness on the fatigue resistance and failure location of pipe-to-plate welded joints under bending. International Journal of Fatigue 90, 78–86. doi:10.1016/j.ijfatigue.2016.04.015.

[5] Chiocca, A., Frendo, F., Bertini, L., 2019a. Evaluation of Heat Sources for the Simulation of the Temperature Distribution in Gas Metal Arc Welded Joints. Metals 9, 1142. doi:10.3390/met9111142.

[6] Chiocca, A., Frendo, F., Bertini, L., 2019b. Evaluation of residual stresses in a tube-to-plate welded joint. MATEC Web of Conferences 300, 19005. doi:10.1051/matecconf/201930019005.

[7] Clarin, M., 2004. High strength steel : local buckling and residual stresses.

[8] Farajian, M., Nitschke-Pagel, T., Boin, M., Wimpory, R.C., 2013. Relaxation of welding residual stresses in tubular joints under multiaxial loading. The Tenth International Conference on Multiaxial Fatigue & Fracture (ICMFF10) .

[9] Frendo, F., Bertini, L., 2015. Fatigue resistance of pipe-to-plate welded joint under in-phase and out-of-phase combined bending and torsion. International Journal of Fatigue 79, 46–53. doi:10.1016/j.ijfatigue.2015.04.020.

[10] Frendo, F., Marulo, G., Chiocca, A., Bertini, L., 2020. Fatigue life assessment of welded joints under sequences of bending and torsion loading blocks of different lengths. Fatigue & Fracture of Engineering Materials & Structures 43, 1290–1304. doi:10.1111/ffe.13223.

[11] Guo, J., Fu, H., Pan, B., Kang, R., 2019. Recent progress of residual stress measurement methods: A review. Chinese Journal of Aeronautics doi:10.1016/j.cja.2019.10.010.

[12] Kainuma, S., Yang, M., Jeong, Y.S., Inokuchi, S., Kawabata, A., Uchida, D., 2017. Experimental investigation for structural parameter effects on fatigue behavior of rib-to-deck welded joints in orthotropic steel decks. Engineering Failure Analysis 79, 520–537. doi:10.1016/j.engfailanal.2017.04.028.

[13] Lee, J.M., Seo, J.K., Kim, M.H., Shin, S.B., Han, M.S., Park, J.S., Mahendran, M., 2010. Comparison of hot spot stress evaluation methods for welded structures. International Journal of Naval Architecture and Ocean Engineering 2, 200–210. doi:10.2478/ijnaoe-2013-0037.

[14] Li, T., Zhang, L., Chang, C., Wei, L., 2018. A Uniform-Gaussian distributed heat source model for analysis of residual stress field of S355 steel T welding. Advances in Engineering Software 126, 1–8. doi:10.1016/j.advengsoft.2018.09.003.

[15] Montanari, R., Fava, A., Barbieri, G., 2018. Experimental Techniques to Investigate Residual Stress in Joints, in: Residual Stress Analysis on Welded Joints by Means of Numerical Simulation and Experiments. InTech. doi:10.5772/intechopen.71564.

[16] Nguyen, T., Wahab, M., 1998. The effect of weld geometry and residual stresses on the fatigue of welded joints under combined loading. Journal of Materials Processing Technology 77, 201–208. doi:10.1016/s0924-0136(97)00418-4.

[17] Vanboven, G., Chen, W., Rogge, R., 2007. The role of residual stress in neutral pH stress corrosion cracking of pipeline steels. part i: Pitting and cracking occurrence. Acta Materialia 55, 29–42. doi:10.1016/j.actamat.2006.08.037.

[18] Xiang, Y., Teng, D., Deng, M., Li, Y., Liu, C., Xuan, F., 2018. Characterization of local residual stress at blade surfaces by the v(z) curve technique. Metals 8, 651. doi:10.3390/met8080651.

[19] Xu, C., Song, W., Pan, Q., Li, H., Liu, S., 2015. Nondestructive testing residual stress using ultrasonic critical refracted longitudinal wave. Physics Procedia 70, 594–598. doi:10.1016/j.phpro.2015.08.030.

[20] Zarandi, E.P., Skallerud, B.H., 2020. Experimental and numerical study of mooring chain residual stresses and implications for fatigue life. International Journal of Fatigue 135, 105530. doi:10.1016/j.ijfatigue.2020.105530.

[21] Zheng, B., Yang, S., Jin, X., Shu, G., Dong, S., Jiang, Q., 2020. Test on residual stress distribution of welded s600e high-strength stainless steel sections. Journal of Constructional Steel Research 168, 105994. doi:10.1016/j.jcsr.2020.105994.